Modulation of auroral electrojet currents using dual modulated HF beams with ELF phase offset, a potential D-region ionospheric diagnostic

M. Gołkowski,[1] M. B. Cohen,[2] and R. C. Moore[3]

Received 17 January 2013; revised 7 March 2013; accepted 12 March 2013.

[1] Experiments at the ionospheric heating facility of the High Frequency Active Auroral Research Program (HAARP) are performed employing dual HF beams amplitude modulated at ELF/VLF with a phase offset between the two modulation waveforms. The amplitude of the observed ELF/VLF waves is strongly dependent on the imposed ELF/VLF phase offset, the modulation waveform, and the orientation of the HF beams. Data from two ground stations are interpreted using simulations of modulated heating power envelopes as well as a comprehensive model of ionospheric ELF/VLF generation. It is found that two colocated vertical beams HF beams excite a single ionospheric ELF/VLF source, but independent ELF/VLF sources can be induced in the ionospheric region above the heater if the HF beams are offset from zenith to intersect at their 3 dB points. Furthermore, the use of two vertical HF beams with ELF phase offset is found to be a potential diagnostic method for the ionospheric D region.

Citation: Gołkowski, M., M. B. Cohen, and R. C. Moore (2013), Modulation of auroral electrojet currents using dual-modulated HF beams with ELF phase offset, a potential D-region ionospheric diagnostic, *J. Geophys. Res. Space Physics*, *118*, doi:10.1002/jgra.50230.

1. Introduction

[2] The ionospheric heating facility of the High Frequency Active Auroral Research Program (HAARP) in Gakona, Alaska (62.4°N and 145.2°W) has been actively used to generate ELF/VLF (3 Hz–30 kHz) radiation by modulation of the overhead auroral electrojet currents for more than a decade [*Papadopoulos et al.*, 2003; *Moore et al.*, 2007; *Cohen et al.*, 2008a, 2008b; *Fujimaru and Moore*, 2011; *Gołkowski et al.*, 2011; *Cohen et al.*, 2012]. Since 2007, the HAARP facility has been capable of radiating 3.6 MW of HF power in the 2.75—10 MHz band. Due to the relatively low conversion efficiency of HF to ELF/VLF power of around 0.001% [*Moore*, 2007], various techniques have been investigated theoretically and experimentally to improve and understand the efficiency and directionality of ELF/VLF generation. These techniques have included heating with HF beams at oblique angles [*Barr et al.*, 1988], rapid motion of a CW HF beam [*Cohen et al.*, 2008b, 2010], special preheating of the ionospheric plasma [*Milikh and Papadopoulos*, 2007],and employing dual HF beams [*Moore and Agrawal*, 2011]. Furthermore, generation conditions are strongly affected not only by the presence of electrojet currents but also the plasma density gradients in the D region [*Jin et al.*, 2009, 2011]. While the electrojet currents can be estimated, at least to first order, using magnetometers, the D-region profile is more difficult to quantify in real time.

[3] Here we describe a novel set of experiments employing two amplitude modulated (AM) HF beams with ELF/VLF phase offset. This work expands upon previous heating experiments where the ELF/VLF phasing was not directly imposed but resulted from the nature of the experiment. At the Tromsø facility, a series of experiments described by *Barr et al.* [1987, 1988] involved an off-zenith HF beam in which the finite propagation delay of HF heating waves to ionospheric altitudes creates ELF/VLF phase shifts along the heated region. The initial experiment design for this work was motivated by the results of *Cohen et al.* [2008b, 2010] in which, under what is known as "geometric modulation," a virtual horizontal phased array is created by CW HF beam motion. A key question has been the coherence length of ionospheric current modulation, and to what extent, heated regions of the ionosphere can be treated as independent ELF/VLF sources. Here the possibility of creating a two element array with operator-imposed phasing was investigated using two colocated beams and also two separated beams. We interpret observed data using simulations of modulated heating power envelopes as well as a comprehensive model of the ionospheric ELF/VLF generation.

[1]Department of Electrical Engineering, University of Colorado Denver, Denver, Colorado, USA.
[2]Directorate for Engineering Division of Electrical, Communications and Cyber Systems, National Science Foundation, Washington, District of Columbia, USA.
[3]Department of Electrical Engineering, University of Florida, Gainesville, Florida, USA.

Corresponding author: M. Gołkowski, Department of Electrical Engineering, University of Colorado Denver, Campus Box 110, 1200 Larimer St. P.O. Box 173364, Denver, CO 80217 94305, USA. (mark.golkowski@ucdenver.edu)

2169-9380/13/10.1002/jgra.50230

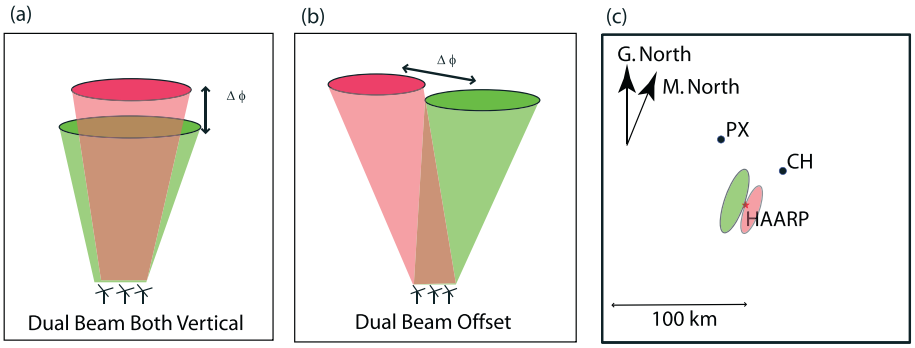

Figure 1. Cartoon schematic of dual beam experiments with both beams in (a) vertical orientation and (b) offset beams. Figure 1c shows a map of the HAARP vicinity and receiver sites as well as approximate beam cross sections at an altitude of 80 km.

For convenience, in the remainder of this report, we will use the acronym "ELF" in place of "ELF/VLF" even though the discussion pertains to modulation frequencies as high as 4 kHz.

2. Experiment and Observations

[4] A cartoon schematic of the overall experiment is shown in Figures 1a and 1b. Several variations of the experiment were performed involving different combinations of HF frequencies and polarizations (O and X mode), distribution of HF dipole elements per beam, square or sinusoidal modulation waveforms, and orientations of the HF beams. We make further distinction between both beams being modulated at the same ELF frequency, which we call "direct phasing" and modulating the second beam at twice the frequency of the first beam, which we call "indirect phasing." The specific parameters for performed Experiments A–D are shown in Table 1. The transmitted values of ω for each experiment were $2\pi \times (2080, 4060,$ and 6040 Hz). The ELF phase offsets discussed in this work are referenced to the ELF modulation shown in Table 1 with the variable ϕ. For the "Offset" orientation (Figure 1b), the two beams were moved symmetrically off zenith to intersect at their 3 dB points. The HAARP HF facility consists of a crossed dipole array of 12×15 elements. When dividing the array into two subarrays to drive dual HF beams, at least one row of 15 dipoles needs to be inactive to provide sufficient HF isolation.

[5] Ionospherically generated ELF waves were observed using magnetic loop antennas at two locations, Chistochina (CH) and Paxson (PX) at 36 km and 51 km distances from HAARP as shown in Figure 1c. Data were recorded using ELF/VLF receivers of the type described by *Cohen et al.* [2009a]. The primary method of ELF data analysis is to observe the generated ELF amplitude as a function of the imposed ELF phase offset. For direct phasing, the amplitude of the fundamental modulated frequency of both beams is analyzed, while for indirect phasing, the amplitude of interest is the second harmonic of the modulation on the first beam and the fundamental of the second beam. Modulation waveforms at HAARP are defined with respect to modulation of HF voltage, but it is the envelope of the HF power that controls the periodicity of ionospheric electron temperature. Thus, what is called sinusoidal modulation at HAARP results in a power modulation of

$$s(t) = \left[\frac{1}{2}\sin(\omega t) + \frac{1}{2}\right]^2. \quad (1)$$

Square wave modulation results in a power envelope given by

$$s(t) = \left[\frac{1}{2}\text{square}(\omega t) + \frac{1}{2}\right]^2, \quad (2)$$

where "square" is the standard odd function periodic square wave of variable duty cycle.

[6] Before discussing specific results, we make the following general remarks on the observations including those made from variations of the transmission formats listed in Table 1. No significant differences were noted in using X mode versus O mode HF polarization. Increasing the HF separation between the two beams by increasing the HF frequency of the second beam toward 9.4 MHz did not yield favorable results due to the lower D-region absorption (and hence minor effect) of the 9.4 MHz frequency

Table 1. Parameters for Dual Beam Experimental Formats Including Carrier Frequency and Polarization (HF), Number of Dipole Elements (Array), and ELF Amplitude Modulation Waveform (AM) for Each Beam[a]

Exp.	HF1	Array1	AM1	HF2	Array2	AM2	Beam Geom.
A	2.75 MHz-X	4×15	Sinusoidal$\left(\frac{\omega}{2}t+\phi\right)$	4.8 MHz-X	7×15	50% square(ωt)	Both vertical
B	2.75 MHz-X	3×15	25% square$\left(\frac{\omega}{2}t\right)$	5.8 MHz-O	8×15	50% square ($\omega t+\phi$)	Both vertical
C	2.75 MHz-X	5×15	sinusoidal$\left(\frac{\omega}{2}t\right)$	5.8 MHz-O	6×15	50% square ($\omega t+\phi$)	Both vertical
D	2.75 MHz-X	5×15	50% square(ωt)	5.8 MHz-X	6×15	50% square ($\omega t+\phi$)	Offset
A′	2.75 MHz-X	4×15	50% square$\left(\frac{\omega}{2}t+\phi\right)$	4.8 MHz-X	7×15	Sinusoidal(ωt)	Both vertical

[a]Experiment A′ was not transmitted but is discussed as well suited for a D-region diagnostic.

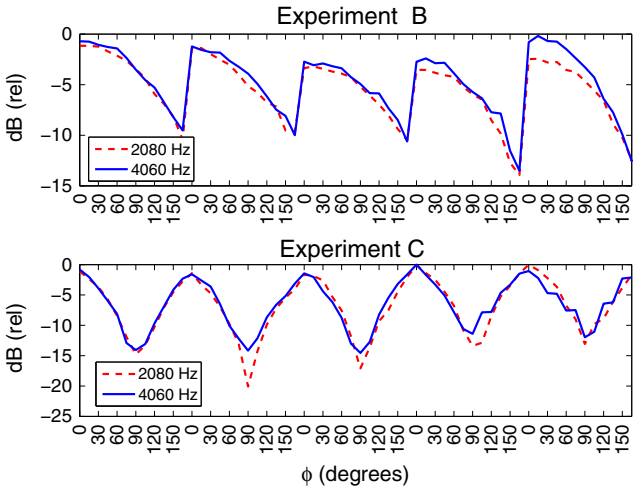

Figure 2. Relative ELF wave amplitude (averaged over 1 s tones) as a function of ELF phase offset ϕ for two different frequencies observed at CH. Top panel shows observations from Experiment B, and bottom panel from Experiment C as defined in Table 1.

HF waves. The modulation waveform (i.e., square wave versus sinusoidal) was found to have a profound effect on the results.

2.1. Colocated Vertical HF Beams

[7] Figure 2 shows data from Experiments B and C showing relative amplitude of ELF waves from both orthogonal antennas at CH at 2080 Hz and 4060 Hz. For both experiments, the ELF phase offset was cycled from 0° to 165° in increments of 15°. We first note that for each experiment, the amplitude as a function of phase is largely the same for both modulation frequencies. This implies that the observations are dominated by the interaction of both HF beams in a single ionospheric region. If the two beams were instead modulating two distinct regions of the ionosphere with finite physical separation, then the ratio of this separation distance to the modulation wavelength would be manifested in the data as an equivalent phase offset. For example, if the two sources were distinct and separated by, say, 10 km, then at 2080 Hz, there would be an additional phase shift of at least 25°, while at 4060 Hz, there would be an additional phase shift of at least 49°. These frequency-dependent phase shifts would produce an offset in the amplitude versus phase pattern for the two frequencies. Since this is not the case, it can be concluded that the primary action of both beams is to modulate the currents in the same ionospheric region. For both experiments, the amplitude maxima occur at 0°, but the minimum for Experiment C occurs at $\sim$ 90°, while for Experiment B occurs at $\sim$ 165°. The phase dependence of the observations results from the effective power modulation and additional nonlinearities resulting from finite (and different) heating and cooling rates of ionospheric electrons. In order to distinguish between the modulation and ionospheric effects, we simulate the expected effect from the power modulation only. We will refer to this analysis of the power envelopes as the "basic model" since it does not include phase effects stemming from finite ionospheric electron heating and cooling rates nor other physical effects. For Experiment B, the net power modulation can be expressed as

$$s_B(t) = B_1\left[\frac{1}{2}\text{square25}\left(\frac{\omega_0}{2}t\right)+\frac{1}{2}\right]^2 + B_2\left[\frac{1}{2}\text{square50}(\omega_0 t+\phi)+\frac{1}{2}\right]^2, \quad (3)$$

where "square25" and "square50" are the 25% and 50% square waves, respectively, and B_1 and B_2 are the arbitrary scale factors. For Experiment C, the net power envelope is

$$s_C(t) = C_1\left[\frac{1}{2}\sin\left(\frac{\omega_0}{2}t\right)+\frac{1}{2}\right]^2 + C_2\left[\frac{1}{2}\text{square50}(\omega_0 t+\phi)+\frac{1}{2}\right]^2. \quad (4)$$

[8] The phase-dependent amplitudes at frequency ω_0 for power envelopes $s_B(t)$ and $s_C(t)$ are shown in Figure 3. These results were obtained by transforming these signals into the frequency domain and taking the component at $\omega = \omega_0$. The amplitude scaling constants were chosen as $B_1 = B_2 = C_2 = 1$ and $C_1 = 4$ so as to match the observed amplitude changes in Figure 2. This scaling implies that the energy deposited by the 2.75 MHz X-mode 5 × 15 subarray beam is roughly four times more than that deposited by the other HF beams used in Experiments B and C as detailed in Table 1. This scaling is in agreement with known greater ionospheric absorption for X mode polarization and lower HF carrier frequencies. Comparing Figures 2 and 3, it is apparent that the gross features are the same, including the general location of minima and maxima. The simulated results are independent of frequency ω_0, while slight differences between the two modulation frequencies are seen in the observed data. To first order, the basic model is able to reproduce the observations of these two experiments.

[9] The simulated results in Figure 3 (from the basic model) represent the effect of undistorted power envelopes, what we would expect to observe if ionospheric electrons would instantaneously heat and cool. The observations in Figure 2, on the other hand, contain the combined effect of the transmitted power envelopes and distortion caused by finite heating and cooling rates, as well as nonlinear

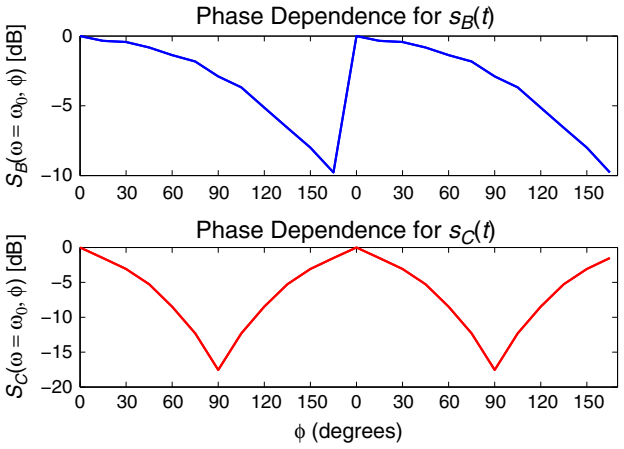

Figure 3. Amplitude at $\omega = \omega_0$ as a function of ϕ for signals $s_B(t)$ and $s_C(t)$ which represent the power envelopes for Experiments B and C using the basic model described in the text.

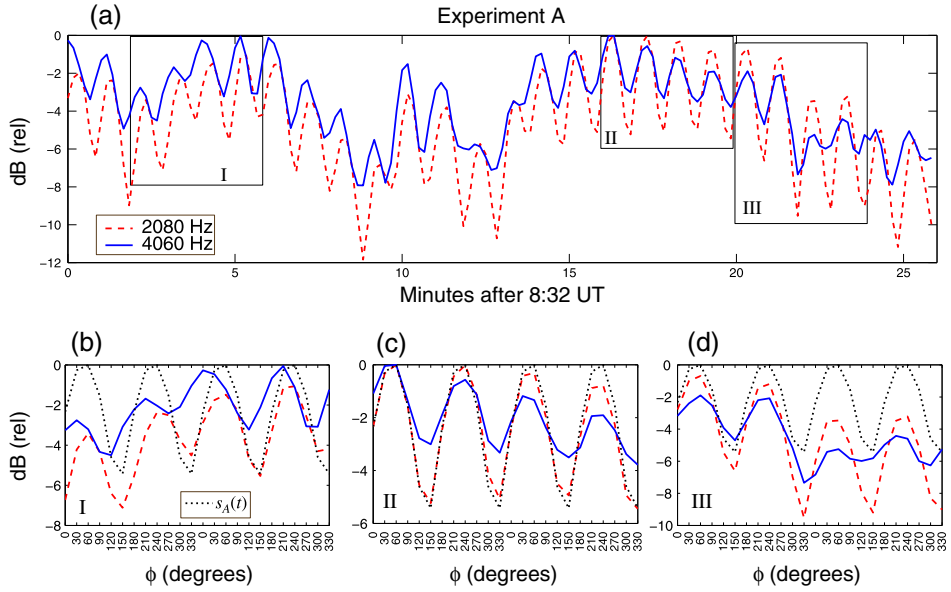

Figure 4. Relative ELF wave amplitude (averaged over 1 s tones) as a function of ELF phase offset ϕ for Experiment A. Figure 4a shows the amplitude of two frequencies observed at CH for 25 min of transmission. Figure 4b shows an expanded scale of the region marked by box I in Figure 4a. Figure 4c shows an expanded scale of the region marked by box II in Figure 4a. Figure 4d shows an expanded scale of the region marked by box III in Figure 4a. The extra dotted trace in Figures 4b–4d is the simulated response for power envelope $s_A(t)$ using the basic model.

HF absorption. The expected effect of these processes on the phase of the effective modulation signal can be seen to derive from the differential equation for electron temperature T_e in the presence of HF heating assuming a Maxwellian distribution:

$$\frac{3}{2}N_e k_B \frac{dT_e}{dt} = 2k\chi S - L_e(T_e, T_0) \tag{5}$$

where N_e is the electron density, k_B is the Boltzmann's constant, k is the HF wave number, χ is the imaginary (absorbing) part of the refractive index calculated from the Appleton-Hartree equation, S is the HF power density, and L_e is a sum of electron loss terms, each a function of T_e and the ambient electron temperature (T_0). Any differential equation with nonzero time constants yields a phase shift of the driver function, which in this case is the HF power envelope. In this case, as the HF power increases, the time derivative of the temperature is positive, and the temperature also increases. However, the temperature increase is not instantaneous and therefore yields a phase shift between the HF power waveform and the electron temperature and thus the ELF fields. This phase shift depends on the heating and cooling time constants which depend on the D-region density. In other words, the waveform distortion from the transmitted power envelope captured by the basic model is frequency and power dependent and affected by the dynamics of D-region density gradients.

[10] The effect of the changing ionospheric conditions can be more clearly seen in the observations from Experiment A shown in Figure 4. Experiment A was run for a longer period of time and had a different phasing pattern. The top panel in Figure 4 shows the amplitudes of two ELF frequencies for 26 min of transmissions during which ϕ was cycled from 0° to 330° in steps of 30° every 10 s. The power profile for this experiment is

$$s_A(t) = A_1\left[\frac{1}{2}\sin\left(\frac{\omega_0}{2}t + \phi\right) + \frac{1}{2}\right]^2 + A_2\left[\frac{1}{2}\text{square50}(\omega_0 t) + \frac{1}{2}\right]^2. \tag{6}$$

[11] Figures 4b, 4c, and 4d show portions of the amplitude data from Figure 4a denoted by boxes I, II, and III as a func-

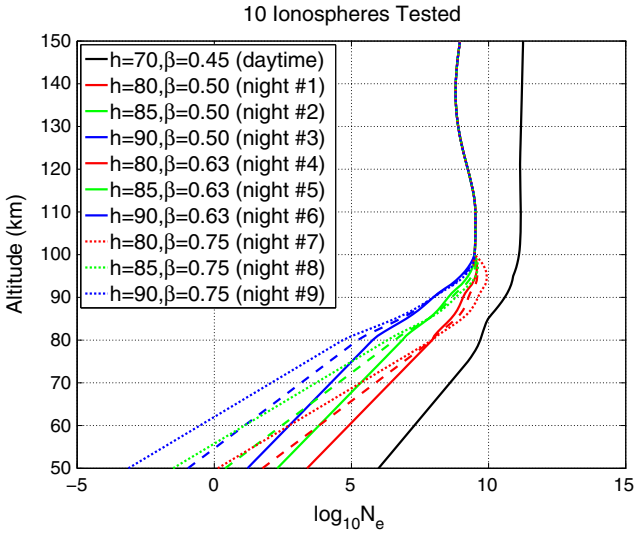

Figure 5. Ionospheric density profiles used in the comprehensive numerical model where h is a reference altitude and β is a gradient coefficient (steepness parameter). For altitudes above 100 km, all profiles are that provided by the International Reference Ionosphere model.

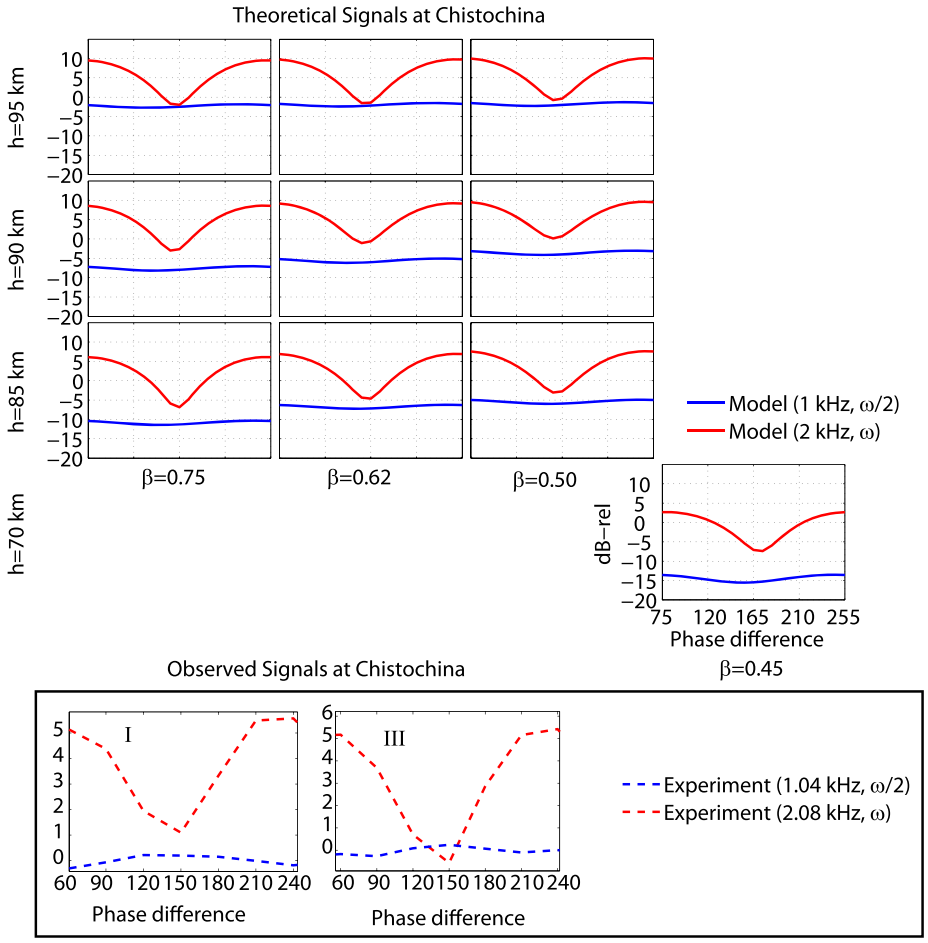

Figure 6. Comprehensive numerical modeling results and select observations from Experiment A.

tion of ϕ. The dotted line in the lower panels is the simulated data using the basic model for the undistorted power envelope $s_A(t)$ for $A_1 = 4, A_2 = 1$. The simulated data is seen to closely match the 2080 Hz observations in Figure 4c . However, the simulated results show marked differences from the observations shown in Figure 4b and 4d in terms of both the location of maxima and minima in phase as well as general shape of the waveforms. For the data in Figures 4b and 4d, the basic model is insufficient to reproduce the observations.

2.2. Potential Ionospheric Diagnostic

[12] Since the shape of the phase-dependent waveform, and more specifically, its departure from that expected from the undistorted power envelope (basic model), is dependent on the D-region conditions, it is feasible to use such waveforms as an ionospheric diagnostic. To validate such an approach, we employ a comprehensive numerical model of the ELF generation process. The modulation of ionospheric currents is modeled using HF ray-tracing and collisional absorption [*Moore*, 2007; *Cohen et al.*, 2010; *Moore and Agrawal*, 2011] involving the numerical solution of equation (5) and calculation of Hall and Pedersen conductivities as a function of time. The propagation of ELF waves from the ionosphere to a ground receiver is modeled using the approach of *Lehtinen and Inan* [2008], which is a full-wave finite element approach. The comprehensive model tracks the heating process with time resolution of 1 μs, and the subsequent simulation of full wave propagation includes both near-field and far-field effects. Thus, the physical processes on all relevant timescales, including those identified by *Papadopoulos et al.* [2005] are taken into account. We note that this comprehensive model has been shown to closely match observations of HAARP-generated ELF waves including copious measurements at the CH site [*Cohen et al.*, 2012]. For given HAARP beam parameters, a D-region ionospheric profile and a receiver location, the comprehensive model is able to predict the phase and amplitude of ELF waves generated in the entire three-dimensional heated region of the ionosphere. To test the dependence on ionospheric profile, we run the model on a set of 10 ionospheric D region electron density profiles of the two parameter form used by *Wait and Spies* [1964] shown in Figure 5. Figure 6 shows the results of the model runs for the different ionospheric profiles parameterized by the scale height h and steepness β for Experiment A for a 2 kHz ELF tone (red curve) and the simultaneously present signal at 1 kHz (blue curve). The minimum as a function of ELF phase ϕ for the red curve and the relative amplitude of the two curves is seen to vary as a function of h and β. The two bottom panels in Figure 6 show corresponding observations from the Experiment A transmission from the time periods demarked I and III in Figure 4. Comparing the model results with the observations (local nighttime), one can conclude that the D-region reference height h increased by approxi-

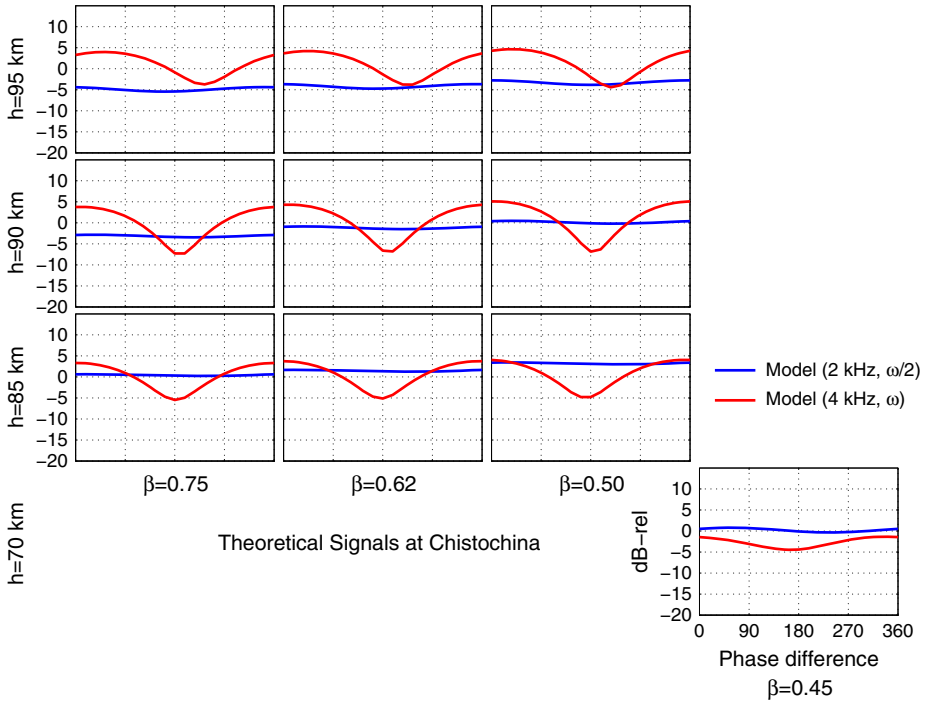

Figure 7. Comprehensive numerical modeling results for improved D region diagnostic for Experiment A′.

mately 10 km over the 20 min duration of Experiment A. Specifically, the amplitude difference between the two frequencies is seen to decrease by $\sim$ 1 dB, which is consistent with a reference height h that is 10 km higher.

[13] The results in Figure 6 show that the Experiment A format has some potential as a D region diagnostic but is far from ideal. Namely, the theoretically expected minimum of the 2 kHz amplitude as a function of phase shows very little variation between the different ionospheric profiles. Figure 7 shows the simulation results for a transmission format identical to Experiment A except that the square and sinusoidal modulations are switched between the two HF beams. This format is denoted as A′ in Table 1. The amplitudes for 2 kHz and 4 kHz ELF waves in Figure 7 show that this modified Experiment A format could serve to uniquely identify an ionospheric D-region profile. For a high value of h, the 2 kHz amplitude is at the minimum of the 4 kHz amplitude; for a low value of h, the 2 kHz amplitude is closer to the maximum of the 4 kHz amplitude. Moreover, the location of the null for the 2 kHz amplitude as a function of phase shifts to the right with increasing ionospheric height. The changes between the relative amplitudes as a function of β (steepness parameter) are more subtle. This is possibly due to the fact that, as can be seen in Figure 5, the effect of β for a constant h is minimal until one descends to altitudes less than $\sim$75 km . It is believed that the dominant interactions for the ELF generation process occur at altitudes of 75–85 km for nighttime conditions [*Stubbe et al.*, 1982; *James*, 1985; *Rietveld et al.*, 1986; *Fujimaru and Moore*, 2011] thus making the β parameter less significant. At the same time, it is important to remember that the actual ionospheric profile can, of course, have features richer than the two-parameter parametrizations shown in Figure 5.

[14] The Experiment A′ format modeled in Figure 7 was not transmitted by HAARP during any of the experiments but will be attempted in the future along with finer increments of the ELF phase and refinement of the ionospheric input profile to better match the observations. It is worth noting that even a first-order approximation of the D region conditions obtainable from a few minutes of HAARP transmissions would provide a useful new capability. The ionospheric D region is notoriously hard to diagnose because the low plasma densities relative to higher ionospheric layers preclude direct radio sounding. At the same time, even small changes in the D-region density gradients can create perturbations in HF wave propagation of the type used in HAARP heating experiments. The diagnostic technique proposed here is based on the nonlinear deformation of the modulated waveform and its harmonics caused by the physics of electron collisional heating and cooling. The collisional heating and cooling rates are functions of plasma density and its gradients. The observation of amplitude as a function of ELF phase provides a measurement relatively impervious to noise as the difference between maxima and minuma is observed on the order of 10 dB. Although it is possible to get the same information by carefully analyzing the amplitude and phase of harmonics of tones generated by modulation from a single HAARP beam, the dual beam technique is simpler and easier to implement since it requires observation at a single ELF frequency and can be accomplished with an amplitude measurement only.

2.3. Offset HF Beams

[15] We now discuss the results of Experiment D where the two HF beams were offset at 3 dB points as shown in Figure 1c. Figure 8 shows the ELF amplitudes observed

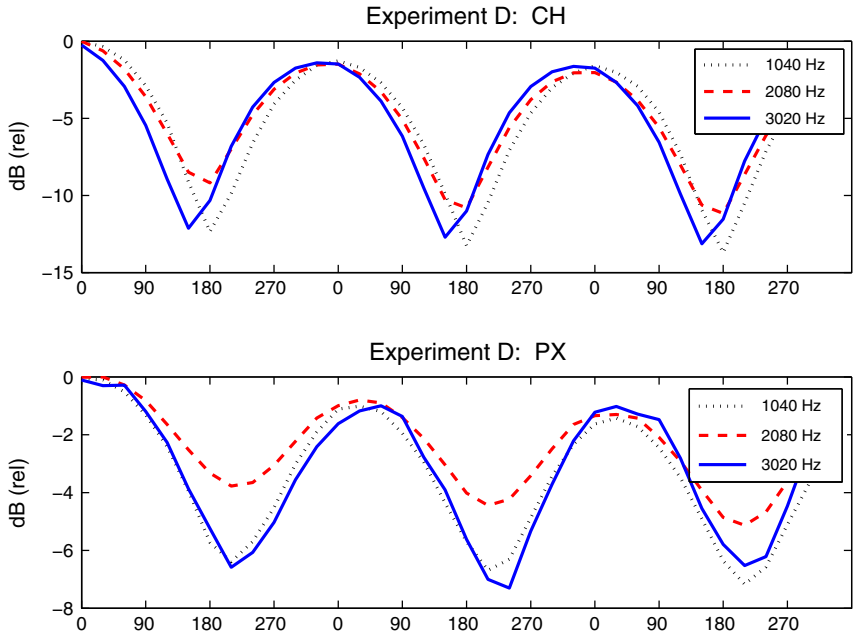

Figure 8. ELF wave amplitude (averaged over 1 s tones) at CH and PX as a function of ELF phase offset ϕ for Experiment D.

at CH and PX as a function of ELF phase. The main distinguishing feature is that the minima and maxima are frequency dependent unlike the case of Experiments A–C. There is an additional difference between the observations at the two sites which are located at different azimuths as shown in Figure 1. The frequency and azimuth dependence suggest the ionospheric current distribution acts like a classic phased array structure with independent sources. In order to assess if the observations are consistent with that of independent sources, an array factor calculation was performed treating patches of the ionosphere heated by each HF beam as independent sources. The HF beam pattern with radiated Poynting flux as a function of angle was obtained with a 1° resolution for each HF beam in Experiment D. Only the parts of the beam within the 3 dB points were considered as shown in Figure 9a. Each pixel of this two-dimensional pattern in Figure 9a is treated as an independent source with an array factor, AF, referenced to the vertical position as

$$\mathrm{AF} = \sum_{n=1}^{N} \left[P_1^n e^{j(\mathrm{kr}^n + \psi_{\mathrm{HF}}^n)} + D P_2^n e^{j(\mathrm{kr}^n + \psi_{\mathrm{HF}}^n + \phi)} \right], \tag{7}$$

where kr^n is the phase from the position of each element, ψ_{HF}^n is the phase from propagation delay of the HF heating waves, and ϕ is the imposed ELF phase on the second beam.

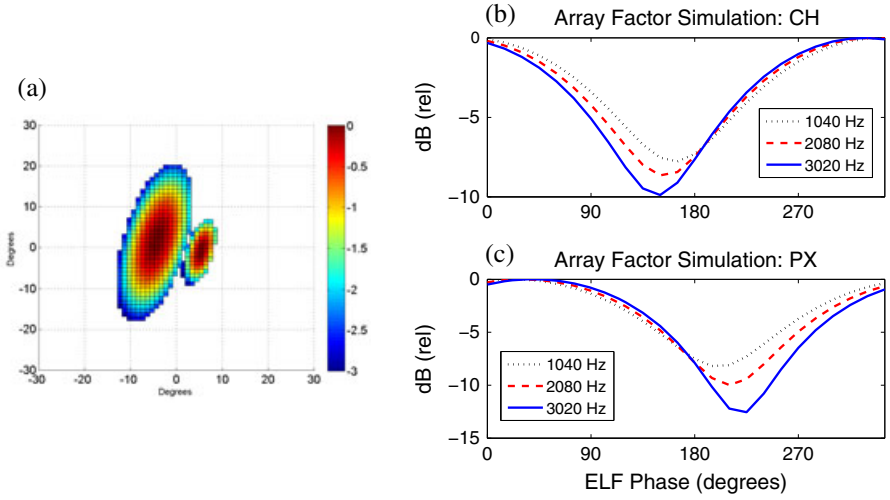

Figure 9. (a) Cross section of HF beam pattern for Experiment D showing intersection of HF beams at 3 dB points. The 2.75 MHz beam is the larger one. (b and c) Array factor calculations for amplitudes expected to be observed at CH and PX as a function of phase offset ϕ.

The first term in the summation is thus the phase accumulated by the ionospheric elements excited by the 2.75 MHz beam scaled by the appropriate Poynting flux P_1^n, and the second term is the accumulated phase, appropriately scaled, of the 5.8 MHz beam of Experiment D. The parameter D is a scale factor used to compensate for the difference in absorption between the two beams that is a function of the HF carrier. The ionospheric sources were assumed to exist at an altitude of 82 km, and the wave number k was calculated assuming a plasma density of $N_e = 10^{9.5}$ m^{-3} and geomagnetic field of 54 μT. Equation (7) is setup to consider monochromatic (sinusoidal) sources, but in our analysis, we used the accumulated phase and amplitude to drive sources modulated with a 50% square wave power envelope that was used in the actual experiment as discussed in the previous section.

[16] Figures 9b and 9c show the results of the array factor calculation for ELF amplitudes expected at CH and PX. Comparing the curves to the observations in Figure 8, it is seen that there is a gross similarity in terms of minima at CH occurring for $\phi < 180°$ and for $\phi > 180°$ at PX for all frequencies. The 3020 Hz amplitude curve at PX exhibits the most similarity between the observations and array factor calculations. It is likely that the observations of 2080 Hz are affected by waveguide resonance effects [*Stubbe et al.*, 1982] near this frequency that are not taken into account in the array factor calculation.

[17] The array factor calculation is of course a significant simplification of the ionospheric generation process and ignores many factors including the overlap of the beams outside of the 3 dB points. This simplified calculation is employed here strictly to isolate the phased array aspect of the ionospheric generation process under the parameters in Experiment D and facilitate identification of features in the observations. The gross similarities between Figure 8 and Figure 9b and 9c lead to the conclusion that to first order, one can consider regions of the ionosphere modulated by HF waves as independent ELF sources.

3. Discussion and Summary

[18] The dual beam phasing experiments described herein give unique access to the subtle distortion of the HF heating power envelope that occurs in the ionospheric D region during heating experiments. The nonlinear absorption of the ionospheric plasma modifies the Fourier spectrum of the transmitted HF signal. *Moore et al.* [2006] investigated the related effect of electron temperature saturation by analyzing the relative amplitude of harmonics of tones generated by modulation from a single HAARP beam. The dual beam technique used here has the advantages that harmonic distortion can be monitored with observation at a single ELF frequency and relative phase of harmonics is accessible through an amplitude measurement of the composite waveform.

[19] The findings of this work can be summarized as follows:

[20] 1. When two HF beams are both oriented vertically, the primary action of both beams is to heat the same ionospheric region, even if the carrier frequency of the second beam is twice that of the first. It does not seem feasible to create a phased array type structure in the vertical direction by selectively heating a desired altitude.

[21] 2. When two HF beams are both oriented vertically, the net modulation of electrojet currents is that of the sum of the power envelopes of both beams to first order. Deviation from the power envelope sum as a function of phase is caused by the specifics of the D-region plasma gradients. The deviations can be modeled and used as a D region diagnostic.

[22] 3. When two HF beams are offset from each other, the beams are able to induce independent ELF sources in agreement with earlier work.

[23] The lack of ability to control the altitude of ionospheric electron temperature modulation using HF carrier frequency or X versus O mode polarization confirms the findings of *Fujimaru and Moore* [2011] who found no significant altitude difference for different HF carriers using a time of arrival technique. The ability of HF heating techniques to generate independent ELF sources was a subject of recent discussion in the literature [*Moore and Rietveld*, 2009; *Cohen et al.*, 2009b]. The results shown herein support the claim that subregions of the ionosphere can be treated independently, thus implying a coherence length of conductivity modification smaller than the dimensions of the heated region. The most novel aspect of the presented results is the potential for a real-time D-region diagnostic using imposed ELF phasing. Implementation of such a utility would require experiments with finer and more rapid ELF phase stepping guided by comprehensive modeling.

[24] **Acknowledgments.** This work has been supported by ONR award N0014-09-1-0100 and AFRL award FA9453-11-C-0011 to Stanford University with subaward 27239350-50917-B to CU Denver. This work is also supported by NSF grants AGS-0940248 and ANT-0944639, ONR grant N000141010909, DARPA contract HR0011-09-C-0099, and DARPA grant HR0011-10-1-0061 to University of Florida with subaward UF-EIES-1005017-UCD to CU Denver. The HAARP transmissions were made possible as part of two special ELF/VLF campaigns at HAARP, organized by Ed Kennedy and Paul Kossey in 2010 and 2011. We thank Mike McCarrick, David Seafolk-Kopf, and Helio Zwi for the operation of the HAARP facility.

References

Barr, R., M. T. Rietveld, P. Stubbe, and H. Kopka (1987), Ionospheric heater beam scanning: A mobile source of ELF radiation, *Radio Sci.*, *22*, 1076–1083.

Barr, R., M. T. Rietveld, P. Stubbe, and H. Kopka (1988), Ionospheric heater beam scanning: A realistic model of this mobile source of ELF/VLF radiation, *Radio Sci.*, *23*, 379–388.

Cohen, M. B., M. Gołkowski, and U. S. Inan (2008a), Orientation of the HAARP ELF ionospheric dipole and the auroral electrojet, *Geophys. Res. Lett.*, *35*, L02806, doi:10.1029/2007GL032424.

Cohen, M. B., U. S. Inan, and M. Gołkowski (2008b), Geometric modulation: A more effective method of steerable ELF/VLF wave generation with continuous HF heating of the lower ionosphere, *Geophys. Res. Lett.*, *35*, L12101, doi:10.1029/2008GL034061.

Cohen, M. B., U. S. Inan, and E. Paschal (2009a), Sensitive broadband ELF/VLF radio reception with the AWESOME instrument, *IEEE Trans. Geos. Rem. Sens.*, *48*(1), 3–17, doi:10.1109/TGRS.2009.2028334.

Cohen, M. B., U. S. Inan, and M. Gołkowski (2009b), Reply to comment by R. C. Moore and M. T. Rietveld on Geometric modulation: A more effective method of steerable ELF/VLF wave generation with continuous HF heating of the lower ionosphere, *Geophys. Res. Lett.*, *36*, L04102, doi:10.1029/2008GL036519.

Cohen, M. B., U. S. Inan, M. Gołkowski, and N. G. Lehtinen (2010), On the generation of ELF/VLF waves for long distance propagation via steerable HF heating of the lower ionosphere, *J. Geophys. Res.*, *115*, A07322, doi: 10.1029/2009JA015170.

Cohen, M. B., M. Golkowski, N. G. Lehtinen, U. S. Inan, and M. J. McCarrick (2012), HF beam parameters in ELF/ VLF wave generation via modulated heating of the ionosphere, *J. Geophys. Res.*, *117*, A05327, doi:10.1029/2012JA017585.

Fujimaru, S., and R. C. Moore (2011), Analysis of time-of-arrival observations performed during ELF/VLF wave generation experiments at HAARP, *Radio Sci.*, *46*, RS0M03, doi:10.1029/2011RS004695.

Gołkowski, M., M. B. Cohen, D. L. Carpenter, and U. S. Inan (2011), On the occurrence of ground observations of ELF/VLF magnetospheric amplification induced by the HAARP facility, *J. Geophys. Res.*, *116*, A04208, doi:10.1029/2010JA016261.

James, H. G. (1985), The ELF spectrum of artificially modulated D/E-region conductivity, *J. Atmos. Terr. Phys.*, *47*(11), 1129–1142.

Jin, G., M. Spasojevic, and U. S. Inan (2009), Relationship between electrojet current strength and ELF signal intensity in modulated heating experiments, *J. Geophys. Res.*, *114*, A08301, doi: 10.1029/2009JA014122.

Jin, G., M. Spasojevic, M. B. Cohen, U. S. Inan, and N. G. Lehtinen (2011), The relationship between geophysical conditions and ELF amplitude in modulated heating experiments at HAARP: Modeling and experimental results, *J. Geophys. Res.*, *116*, A07310, doi:10.1029/2011JA016664.

Lehtinen, N. G., and U. S. Inan (2008), Radiation of ELF/VLF waves by harmonically varying currents into a stratified ionosphere with application to radiation by a modulated electrojet, *J. Geophys. Res.*, *113*, A06301, doi:10.1029/2007JA012911.

Milikh, G. M., and K. Papadopoulos (2007), Enhanced ionospheric ELF/VLF generation efficiency by multiple timescale modulated heating, *Geophys. Res. Lett.*, *34*, L20804, doi:10.1029/2007GL031518.

Moore, R. C., U. S. Inan, and T. F. Bell (2006), Observations of amplitude saturation in ELF/VLF wave generation by modulated HF heating of the auroral electrojet, *Geophys. Res. Lett.*, *33*, L12106, doi:10.1029/2006GL025934.

Moore, R. C. (2007), ELF/VLF wave generation by modulated HF heating of the auroral electrojet, Ph.D. thesis, Stanford Univ., Stanford, Calif.

Moore, R. C., U. S. Inan, T. F. Bell, and E. J. Kennedy (2007), ELF waves generated by modulated HF heating of the auroral electrojet and observed at a ground distance of ∼4400 km, *J. Geophys. Res.*, *112*, A05309, doi:10.1029/2006JA012063.

Moore, R. C., and M. T. Rietveld (2009), Comment on Geometric modulation: A more effective method of steerable ELF/VLF wave generation with continuous HF heating of the lower ionosphere by M. B. Cohen, U. S. Inan, and M. Golłkowski, *Geophys. Res. Lett.*, *36*, L04101, doi:10.1029/2008GL036002.

Moore, R. C., and D. Agrawal (2011), ELF/VLF wave generation using simultaneous CW and modulated HF heating of the ionosphere, *J. Geophys. Res.*, *116*, A04217, doi:10.1029/2010JA015902.

Papadopoulos, K., T. Wallace, M. McCarrick, G. M. Milikh, and X. Yang (2003), On the efficiency of ELF/VLF generation using HF heating of the auroral electrojet, *Plasma Phys. Rep.*, *29*, 561–565

Papadopoulos, K., T. Wallace, G. M. Milikh, W. Peter, and M. McCarrick (2005), The magnetic response of the ionosphere to pulsed HF heating, *Geophys. Res. Lett.*, *32*, L13101, doi:10.1029/2005GL023185.

Rietveld, M. T., H. Kopka, and P. Stubbe (1986), D-region characteristics deduced from pulsed ionospheric heating under auroral electrojet conditions, *J. Atmos. Terr. Phys.*, *48*(4), 311–326.

Stubbe, P., H. Kopka, M. T. Rietveld, and R. L. Dowden (1982), ELF and VLF wave generation by modulated HF heating of the current carrying lower ionosphere, *J. Atmos. Terr. Phys.*, *44*, 1123–1135

Wait, J. R., and K. P. Spies (1964), Characteristics of the Earth ionosphere waveguide for VLF radio waves. Tech Note 300, Nat'l Bur. of Stand., Boulder, Colo.